Article

Effects of theTiB₂-SiC Volume Ratio and Spark Plasma Sintering Temperature on the Properties and Microstructure of TiB₂-BN-SiC Composite Ceramics

Shi Tian [1], Zelin Liao [1], Wenchao Guo [1], Qianglong He [1], Heng Wang [2,*] and Weimin Wang [1,*]

[1] The State Key Laboratory of Advanced Technology for Materials Synthesis and Processing, Wuhan University of Technology, Wuhan 430070, China; shitian@whut.edu.cn (S.T.); liaozelin1702@whut.edu.cn (Z.L.); whutguowc@whut.edu.cn (W.G.); shsqlhe@whut.edu.cn (Q.H.)

[2] Hubei Key Laboratory of Plasma Chemistry and Advanced Materials, Key Laboratory of Green Chemical Engineering Process of Ministry of Education, Wuhan Institute of Technology, Wuhan 430205, China

* Correspondence: wangheng@wit.edu.cn (H.W.); shswmwang@whut.edu.cn (W.W.)

Abstract: TiB₂-BN composite ceramics combine excellent electrical conductivity, thermal shock resistance, high-temperature resistance, corrosion resistance, and easy processing of TiB₂ and BN. However, in practical applications, their high-temperature oxidation resistance is poor and the resistivity distribution is uneven and changes substantially with temperature. A TiB₂-BN-SiC composite ceramic with stable and controllable resistivity was prepared by introducing SiC into the TiB₂-BN composite ceramics. In this work, spark plasma sintering (SPS) technology was used to prepare TiB₂-BN-SiC composite ceramics with various TiB₂-SiC ratios and sintering temperatures. The samples were tested by XRD, SEM, and thermal and mechanical analysis. The results show that as the volume ratio of TiB₂-SiC was increased from 3:1 to 12:1, the resistivity of the sample decreased from 8053.3 to 4923.3 μΩ·cm, the thermal conductivity increased from 24.89 to 34.15 W/(m k), and the thermal expansion rate increased from 7.49 (10^{-6}/K) to 10.81 (10^{-6}/K). As the sintering temperature was increased from 1650 to 1950 °C, the density of the sample increased, the mechanical properties were slightly improved, and the resistivity, thermal expansion rate, and thermal conductivity changed substantially. The volume ratio and sintering temperature are the key factors that control the resistivity and thermal characteristics of TiB₂-SiC-BN composite ceramics, and the in situ from liquid phases of FeB and FeO also promotes the sintering of the TiB₂-BN-SiC ceramics.

Keywords: TiB₂-BN-SiC; spark plasma sintering; physical properties; microstructure

1. Introduction

Both TiB₂ and BN have high hardness, high wear resistance, high melting point, and high temperature stability; hence, they are widely used in industrial production, such as in aerospace applications, metal evaporation plating, and wear-resistant coatings [1–5]. TiB₂-BN composite ceramics have the unique properties of both TiB₂ and BN, such as excellent electrical conductivity [6,7] and excellent lubricity to molten metal. Therefore, TiB₂-BN composite ceramics are widely used in the cast aluminum industry [8]. In 2008, Jens Eichler et al. [8] composited BN and ZrO₂ to prepare side dams for use in thin strip casting, which showed satisfactory corrosion resistance, wear resistance, and high-temperature compressive stress. In 2012, by magnetron sputtering, Dong et al. [9] prepared a TiB₂/BN multilayer film with a smaller grain size and a stable layer structure that had a polycrystalline TiB₂ texture with amorphous BN; it showed higher hardness and higher elastic modulus than coatings of only TiB₂ or BN. The study in [10] indicates that McKinnon et al. used flash spark plasma sintering (FSPS) technology to quickly sinter a cold-pressed TiB₂-hBN disc from a powder into an almost-dense material (up to 97%) in less than 110 s. Recently, Bin Song et al. [11] prepared nearly densified samples by doping BN and SiC into TiB₂ powder under hot-press sintering conditions at 2000 °C and 50 MPa. The density

of a ceramic has a larger impact on the mechanical properties and thermal properties of the ceramic and is an important factor in determining the service life of the ceramic. However, the environment of the evaporation plating industry is relatively harsh. Due to the high temperature and the service conditions of contact with molten metal, ceramic boats that contain molten metal in the metal evaporation plating industry need to have high-temperature resistance, corrosion resistance, satisfactory metal compatibility, and stable conductivity [12–14]. Unstable conductivity and a narrow adjustment range will lead to unstable current when the boat is in service, unbalanced boat body temperature, and reduced evaporation efficiency. In addition, uneven resistivity and poor high-temperature thermal stability will also reduce TiB_2, which is an important factor in the working life of BN ceramics. Therefore, the density of ceramics and their thermal and electrical properties are equally important in evaporative aluminum plating.

SiC has high wear resistance, high strength, high hardness, a low thermal expansion coefficient, high thermal conductivity, satisfactory thermal stability at high temperatures, and satisfactory oxidation resistance [15–17]. In addition, adding SiC to a ceramic can improve the material's fracture toughness, oxidation resistance, and controllable conductivity [2,18–21]. In our previous research, TiB_2-BN-SiC composite ceramics were produced using the hot-pressing sintering method, and the progress in sintering technology has made ceramic sintering methods more diverse. In this work, the mechanical alloying method is used to prepare a mixed powder, and the TiB_2-BN-SiC three-phase composite ceramic is prepared by the SPS sintering method, which differs from the hot-pressing sintering method. The relative density, resistivity, and elasticity of the composite ceramic are characterized. The modulus, flexural strength, thermal expansion coefficient, thermal conductivity, and other properties and three test methods, namely, X-ray diffraction (XRD), scanning electron microscope (SEM), and back scattered electron (BSE) are used to analyze the samples, and the changes in the above properties under various TiB_2-SiC ratios and sintering temperatures are studied. This work has reference significance for the preparation and production of ceramics of the same type for high-temperature work.

2. Experimental Procedure

2.1. Preparation of the TiB_2-BN-SiC Composite Powder

TiB_2 powder (Dandong Chemical Engineering Institute, $d_{0.5}$ = 4 μm, oxygen content 0.79%), h-BN powder (Dandong Chemical Engineering Institute, $d_{0.5}$ = 0.6 μm, oxygen content 0.91%), and SiC powder (Shanghai Chaowei Nanotechnology Co., Ltd. $d_{0.5}$ = 0.34 μm, purity >99%) were used as raw material powders. Ethanol was used as a process control agent (PCA), and the addition amount was calculated as a mass percentage of the powder. The volume content of BN was controlled at a constant percentage of 72%, the volume ratio of TiB_2/SiC was changed, and the mixed powder was configured in ratios of 3:1, 6:1, 9:1, and 12:1, as presented in Table 1. The planetary ball milling method [22–24] was used to mix the powder. Weighed steel balls, the mixed powder, and absolute ethanol were added to the ball milling tank in sequence. Then, the ball milling tank was closed and placed into the planetary ball mill (the ball milling tank was a φ90 mm × 80 mm stainless steel tank, the stainless-steel grinding balls had a ratio of φ12 mm:φ6 mm = 1:5, the mass ratio of the stainless-steel balls to the mixed powder was 30:1, the ball mill speed was 300 r/min, and the ball milling time was 2 h). The middle ball mill was completed. Then, the ball mill tank was removed, and the resulting mixed slurry was poured into a rotary evaporator and rotary evaporated. After completion, vacuum drying, grinding, and sieving were carried out to obtain the composite powder.

Table 1. Theoretical volume ratios of TiB$_2$ and SiC.

TiB$_2$-SiC	TiB$_2$ (Vol%)	SiC (Vol%)
3:1	21	7
6:1	24	4
9:1	25.2	2.8
12:1	25.8	2.2

### 2.2. Preparation of TiB$_2$-BN-SiC Multiphase Ceramics

Into a graphite mold, 3.60 g of raw powders with various proportions were placed. The composite powders were separated from the mold and the indenter with graphite paper and placed in an SPS sintering furnace for sintering [25]. During the sintering process, the heating rate was controlled to 100 °C/min, the holding time was 5 min, and the protective atmosphere was Ar. First, the sintering temperature was controlled to 1850 °C, and 3:1, 6:1, 9:1, and 12:1 samples were prepared. Then, the composition was controlled to a constant ratio of 6:1 at 1650, 1750, 1850, and 1950 °C. The samples were prepared separately at the sintering temperature.

2.3. Testing and Characterization

The relative density of the sample was measured by the Archimedes drainage method at room temperature. An ST2258C digital four-probe tester was used to measure the resistivity of the complex phase ceramics, and the distance between the two probes was 0.2 cm.

Figure 1 shows the method and principle of resistivity testing. When four metal probes were arranged in a straight line and touched on the sample with a certain pressure, the current passing between probes 1 and 4 is recorded as Current (I), and the potential difference generated between probes 2 and 3 was marked as Voltage (V). In that case, the resistivity ρ(Ω·cm) of the material can be calculated by following Formula (1):

$$\rho = C \times V/I \tag{1}$$
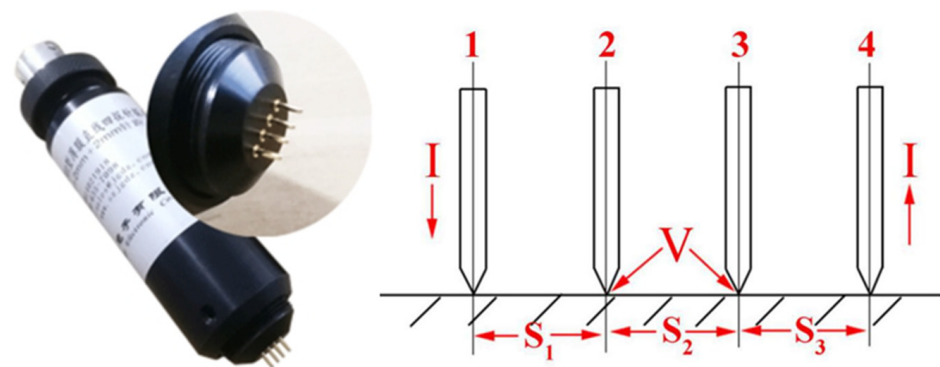
Figure 1. Schematic diagram of resistivity measurement by four-probe method.

In the formula, C is the probe correction coefficient, which is determined by the distance between the probes. When the sample resistance is evenly distributed and the sample size meets the semi-infinity condition, C can be calculated by the following Formula (2).

$$C = \frac{2\pi}{\frac{1}{S1} + \frac{1}{S2} - \frac{1}{S1+S23} - \frac{1}{S2+S3}} \tag{2}$$

In the above formula, *S*1, *S*2, and *S*3, respectively, represent the distances between 1 and 2, 2 and 3, and 3 and 4 in Figure 1. After calculating the resistivity result from the test data, the conductivity value σ(S/m) can be calculated by the following Formula (3):

$$\sigma = \frac{1}{\rho} \qquad (3)$$

The flexural strength of the material and the elastic modulus of the material were measured by the three-point bending method on an MTS-810 ceramic test system, and the loading rate was 0.5 mm/min. A TC-7000H Laser Flash thermal constant analyzer was used to measure the thermal conductivity of the sample; the test temperature was 600 °C, and an Ar atmosphere was used. A NETZSCHDIL402C thermal dilatometer was used to measure the thermal expansion coefficient of the sample. The test temperature ranged from room temperature to 1000 °C in an Ar atmosphere. X-ray diffraction was used to characterize the phase composition of the sample, and the fracture morphology of the sample was observed with a scanning electron microscope (JSM–S3400).

3. Results and Discussion

3.1. Effects of the TiB$_2$-SiC Volume Ratio on the Material Properties, Microstructure, and Phase Composition

In order to better study the effect of the ratio of titanium diboride and silicon carbide on the performance of TiB$_2$-BN-SiC composite ceramics, we controlled the sintering temperature at 1850 °C and explored four ratios of TiB$_2$ and SiC, namely 3:1, 6:1, 9:1, 12:1.

3.1.1. Effects of the TiB$_2$-SiC Volume Ratio on the Material Properties

Figure 2a shows that as the volume ratio of TiB$_2$-SiC increases, the density of the sintered body increases slightly. This is because as the volume content of TiB$_2$ increases, TiB$_2$ grains sinter more easily, and the probability of contact between heterogeneous particles decreases, thereby resulting in fewer pores [26]. Overall, the volume ratio of TiB$_2$-SiC has no significant effect on the relative density of the composite ceramics. According to the images in Figure 2b, the resistivity of TiB$_2$-BN-SiC composite ceramics at room temperature decreases with increasing TiB$_2$-SiC volume ratio. The deviation interval in the figure is measured at various positions of the same sample. For the set of resistivities, the deviation gradually decreases with increasing ratio, thereby indicating that the resistance stability is gradually improved. This is because the mass fractions of the conductive phase (TiB$_2$) and the semiconductor phase (SiC) are increased relative to that of the insulating phase (BN), which promotes the formation of a conductive network and decreases the resistivity. As shown in Figure 2c, with an increase in the volume ratio of TiB$_2$-SiC, the elastic modulus of the sample fluctuates at approximately 84 GPa, the change in the elastic modulus is not obvious, and the flexural strength fluctuates in the range of 180–190 MPa. Figure 2d shows that as the volume ratio of TiB$_2$-SiC increases, the average thermal expansion coefficient increases from 7.5×10^{-6}/K to 10.8×10^{-6}/K, namely, by 44%. In addition, as the volume ratio of TiB$_2$-SiC increases, the thermal conductivity increases from 28.89 to 34.04 W/(m·K). This is because the theoretical thermal conductivity of TiB$_2$ is much higher than that of SiC. As the volume content of TiB$_2$ increases, the crystal structure of the material becomes more perfect, less scattering of lattice waves occurs, the mean free path of phonons increases, and the thermal conductivity increases.
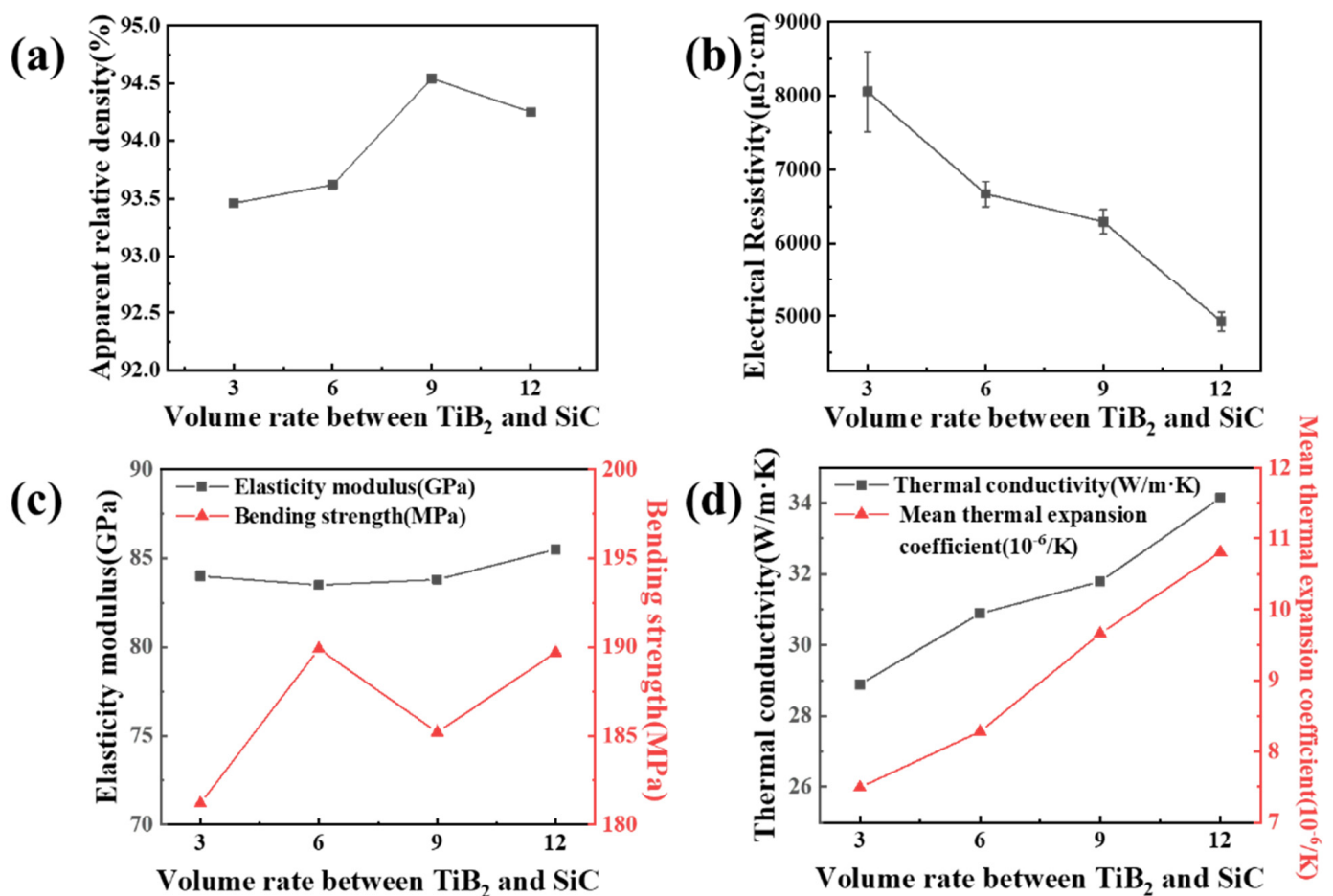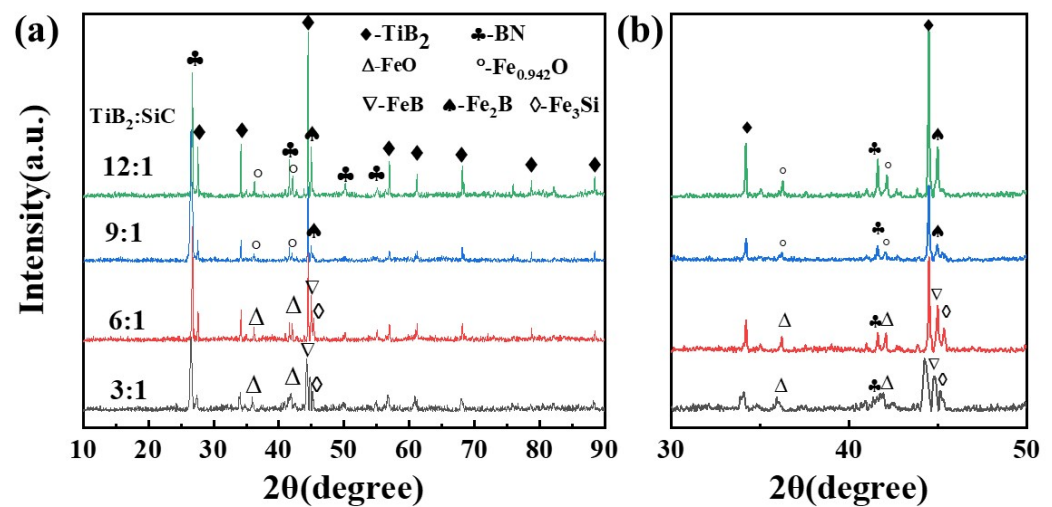
Figure 2. Properties of TiB_2-BN-SiC composite ceramics with various volume ratios of TiB_2-SiC: (**a**) the apparent relative density, (**b**) electrical resistivity, (**c**) elastic modulus and bending strength, and (**d**) thermal conductivity and mean thermal expansion coefficient.

3.1.2. Influence of the TiB_2-SiC Ratio on the Material Phase and Microstructure

Figure 3 shows that the XRD spectra of four samples all show clear diffraction peaks of TiB_2 and BN. As the volume ratio of TiB_2-SiC increases, the peak that corresponds to TiB_2 gradually increases, and the BN peak does not obviously change. The angle of 30–50° of the diffraction pattern was enlarged to better observe the subtle changes of the phase. In the peak region of 35–50°, different impurity peaks are detected with different TiB_2 contents. With increasing TiB_2 content, a transition from the FeO phase to the $Fe_{0.924}O$ phase occurs. This is mainly because the raw material powder wears part of the steel balls under mutual extrusion with the stainless-steel balls in the process of mechanical alloying and, consequently, Fe is introduced; the TiB_2 powder contains impurity oxygen, and with increasing TiB_2 content, the increase in the oxygen impurity content of the mixed powder promotes the transformation of the FeO phase to the oxygen-rich $Fe_{0.924}O$ phase. Fe_3Si peaks are also detected in the two samples with ratios of 3:1 and 6:1, but the peaks are not detected in the samples with ratios of 9:1 and 12:1. The former shows a peak of FeB, while the latter shows a peak of Fe_2B. This is because when the volume ratio of TiB_2 to SiC increases, the relative content of SiC decreases, and the amount of Si element that can react with Fe to form Fe_3Si decreases. Therefore, Fe_3Si is not detected at the ratios of 9:1 and 12:1. The melting points of FeB and Fe_2B are approximately 1600 °C. These impurities form a liquid phase during the sintering process of the ceramic [2,4], which promotes the sintering of the ceramic; this is consistent with the relative density result.

Figure 3. (**a**) XRD patterns of TiB_2-BN-SiC composite ceramics with various TiB_2-SiC volume ratios, (**b**) is their local feature.

Figure 4 shows cross-sectional SEM images of TiB_2-BN-SiC composite ceramics with four volume ratios of TiB_2-SiC. The microstructure of the section is interlaced with large crystal grains and numerous flaky crystals. The lamellar structure crystals are the BN phase, and the granular crystal grains (TiB_2 phase and SiC phase) are dispersed among the flaky BN crystal grains. As the ratio of TiB_2-SiC increases, the granular grains grow significantly. This has the same changing trend as the microstructure of the multiphase ceramics in Van-Huy Nguyen's research [4]. This is because the relative content of the TiB_2 phase increases, the probability of contact between particles in the TiB_2 phase increases, and bonding between TiB_2 particles produces large grains. According to the theory of multiphase ceramic percolation, the increase in TiB_2 large crystal grains reduces the resistivity of the multiphase ceramics and improves the conductivity, which is consistent with the result that the resistivity decreases with increasing ratio of Figure 2b. According to the figure, the fracture mode is dominated by transgranular fracture of flaky BN grains and intergranular fracture of granular TiB_2 and SiC. The growth of TiB_2 grains promotes the mechanical properties of the ceramics [27]. This is because the size of the grains increases and the fracture form of TiB_2 changes from intergranular fracture to partial transgranular fracture and partial intergranular fracture. In addition, because the theoretical thermal expansion coefficient of TiB_2 is much higher than that of SiC and the TiB_2 content increases, the TiB_2 grains in the sample are tightly connected; hence, the overall thermal expansion coefficient of the sample is substantially affected by the volume content of TiB_2 and, thus, the thermal expansion coefficient increases.

Since the volume of the BN phase accounts for 72% and the total volume of the TiB_2-SiC phase accounts for 28%, the pores that are formed by many flaky BN crystals intersecting each other during ceramic sintering are difficult to replace because small amounts of TiB_2 and SiC are completely filled and changed. Therefore, there are many pores, which is the main reason that the relative density (93.5–94.5%) of the sample is not high.

Figure 5 shows surface backscattering photos of TiB_2-BN-SiC composite ceramics with four volume ratios. The grey–white areas in the picture are TiB_2 particles, and the black areas are the BN matrix. As shown in the figure, as the content of TiB_2 increases, the grain size of TiB_2 in the ceramic matrix increases significantly. From Figure 5a–d the grain size increases from 2.61 to 5.08 μm. This is because as the content of TiB_2 increases, the possibility of TiB_2 particles contacting each other is higher, which facilitates bonding during the sintering process, thereby promoting grain growth. According to the figure, as the ratio increases, the number of fine particles on the surface gradually decreases, thereby indicating that the crystallinity is better, which is also evidenced by the finer phase diffraction peaks.
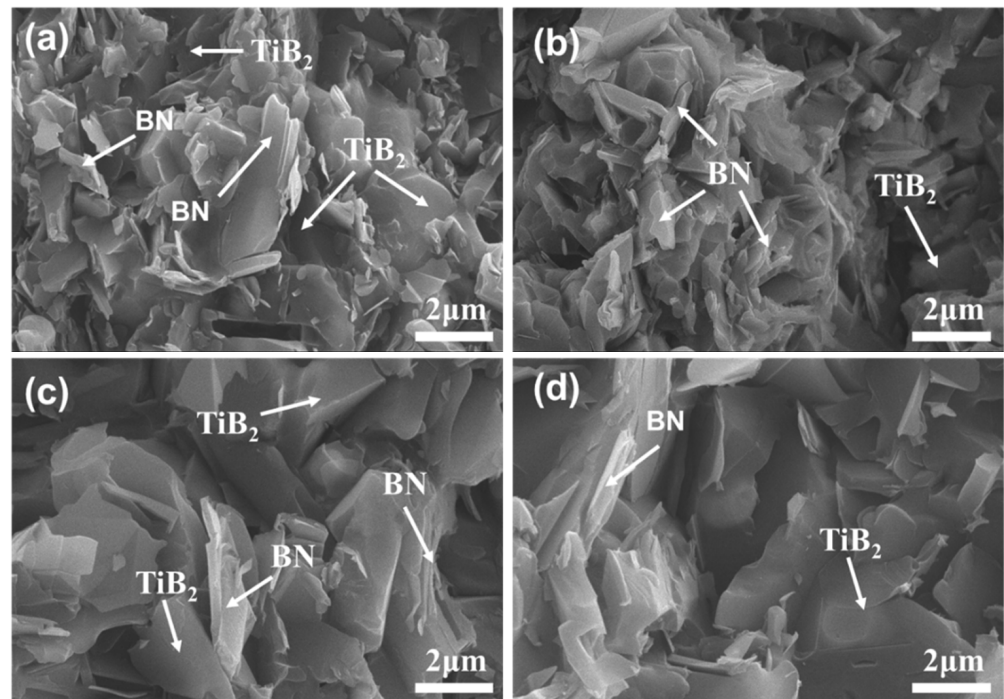
Figure 4. Cross-sectional SEM images of TiB$_2$-BN-SiC composite ceramics with four TiB$_2$-SiC volume ratios: (**a**) 3:1, (**b**) 6:1, (**c**) 9:1, and (**d**) 12:1.
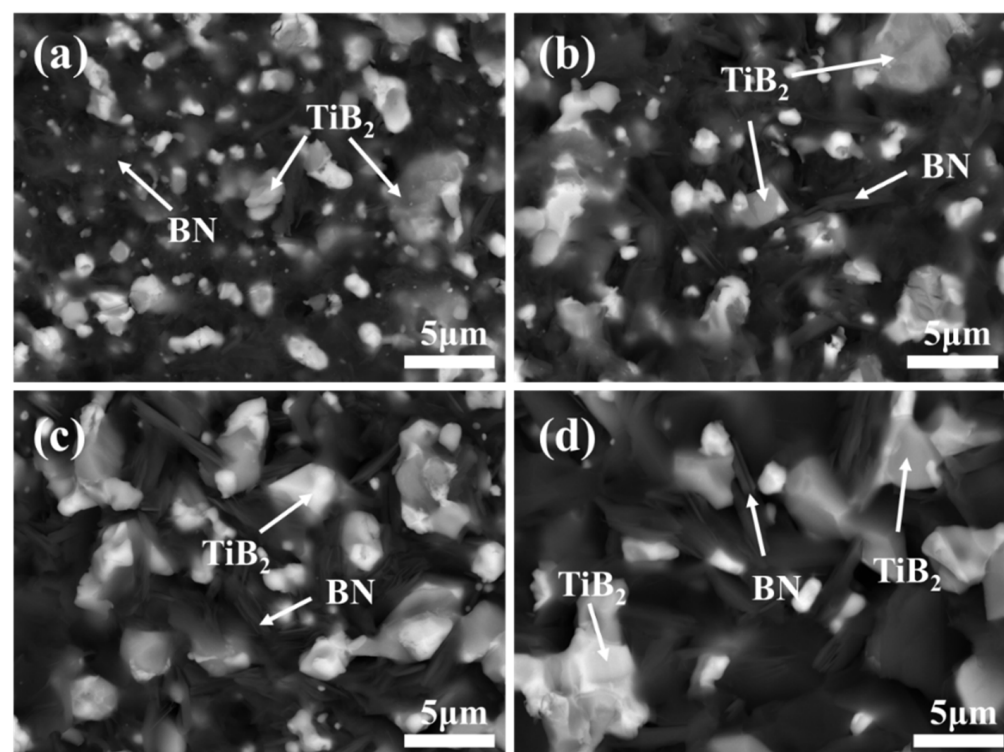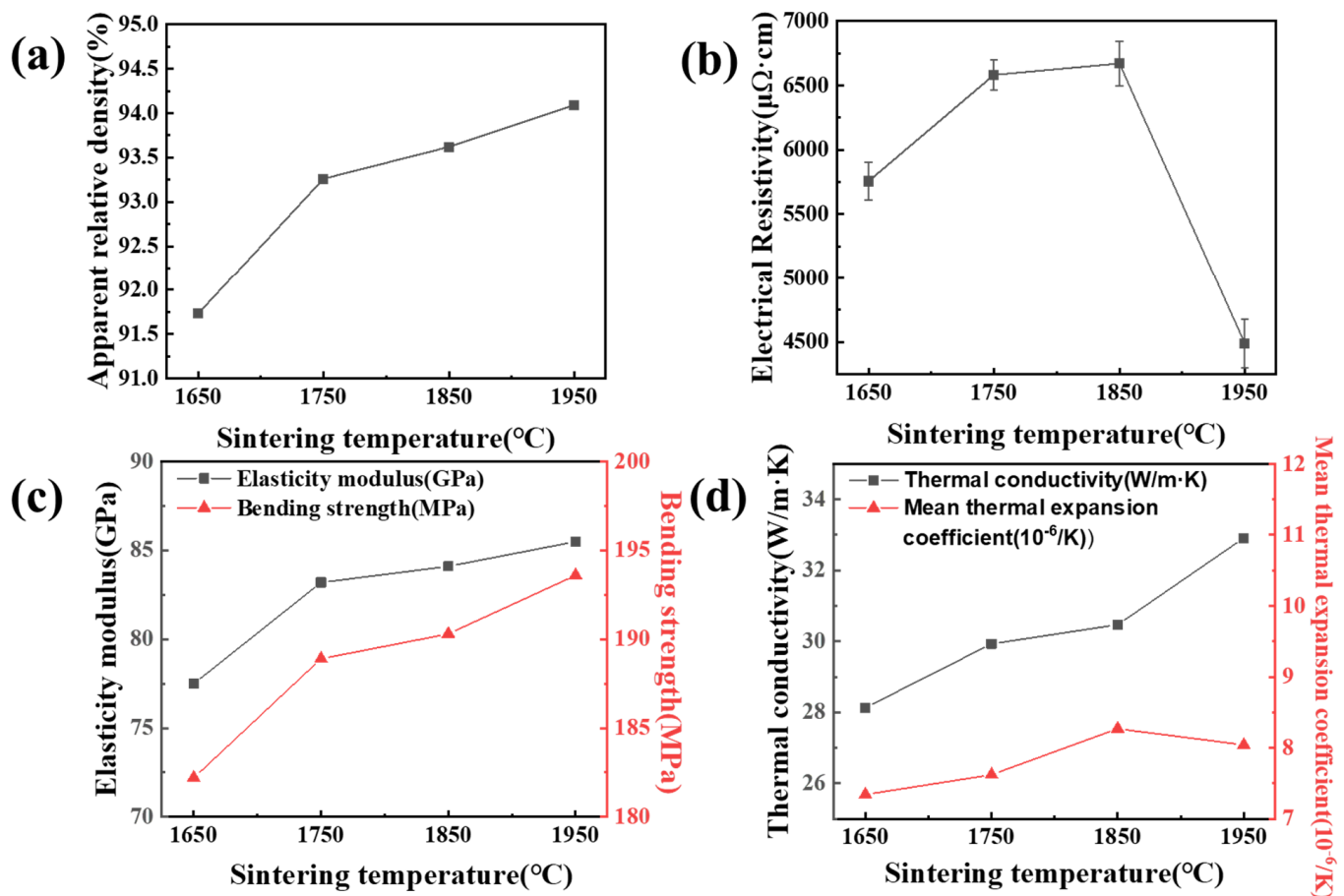

Figure 5. BSE photos of TiB$_2$-BN-SiC composite ceramics with four TiB$_2$-SiC volume ratios: (**a**) 3:1, (**b**) 6:1, (**c**) 9:1, and (**d**) 12:1.

3.2. Effects of the Spark Plasma Sintering Temperature on the Material Properties, Microstructure, and Phase Composition

To further study the effect of sintering temperature on the performance of TiB$_2$-BN-SiC composite ceramics, we explored four temperatures, namely, 1650, 1750, 1850, and 1950 °C, of TiB$_2$ and SiC powders with a volume ratio of 6:1 and examined various properties of the fired block.

3.2.1. Effects of the Sintering Temperature on the Material Properties

According to the images in Figure 6a, when the sintering temperature is increased from 1650 to 1750 °C, the density of the multiphase ceramic sample increases obviously, and when the sintering temperature is increased from 1750 to 1950 °C, the density increases slightly, but the change is not large. Figure 6b shows that with increasing sintering temperature in the range of 1650–1850 °C, the resistivity increases; however, when the temperature reaches 1950 °C, the resistivity decreases. In a previous study, when the author used hot pressing to sinter samples under similar conditions, the resistivity trend was the opposite, namely, a trend of decreasing initially and subsequently increasing was observed [28]. Whereas hot pressing uses an external thermal field to achieve slow energy transfer and uses the surface energy of the material to be densified, SPS uses a large pulse current to conduct rapid sintering, which may be unstable compared with hot pressing. The effects of the sintering temperature on the elastic modulus and flexural strength of TiB$_2$-BN-SiC composite ceramics are shown in Figure 6c. As shown in the figure, as the sintering temperature increases, the flexural strength and elastic modulus both increase. When the sintering temperature is 1650 °C, the elastic modulus and bending strength are 77.5 GPa and 182.2 MPa, respectively. Up to 1950 °C, the elastic modulus value is 85.5 GPa, and the bending strength value is 193.6 MPa. They increase by 10.3% and 6.3%, respectively. Figure 6d shows the effect of the sintering temperature on the thermal conductivity of TiB$_2$-BN-SiC composite ceramics. When the sintering temperature is 1650, 1750, and 1850 °C, the thermal expansion coefficients of the samples are 7.3×10^{-6}, 7.6×10^{-6}, and 8.3×10^{-6}, respectively. As the sintering temperature increases, the thermal expansion coefficient of the sample increases, and the density of the sample increases. The slight decrease in the thermal expansion coefficient at 1950 °C may be due to the very tight bonding between the ceramic powders, which reduces the increase in the amplitude of the lattice vibration when the temperature is increased, thereby macroscopically reducing the thermal expansion. When the sintering temperature is increased from 1650 to 1950 °C, the thermal conductivity of the sample increases from 28.1 to 32.9 W/(m·k), namely, by 17.1%. The reason may be that the density of the sample is increased, and the bonding force between the grains is enhanced, which improves the mechanical properties of the sample. The thermal conductivity increases. This is because the grain size increases, the grain boundaries and pore defects are reduced, the density of the sample increases, and the microstructure becomes more complete and uniform, which is beneficial for increasing the mean free path of phonons and increasing the thermal conductivity rate. At 1650 °C, the sample density is significantly lower, the sample has the most pore defects, the scattering of lattice waves increases, the mean free path of phonons decreases, and the resistivity is the highest, which is not conducive to electronic heat conduction; hence, the thermal conductivity is obviously the lowest.
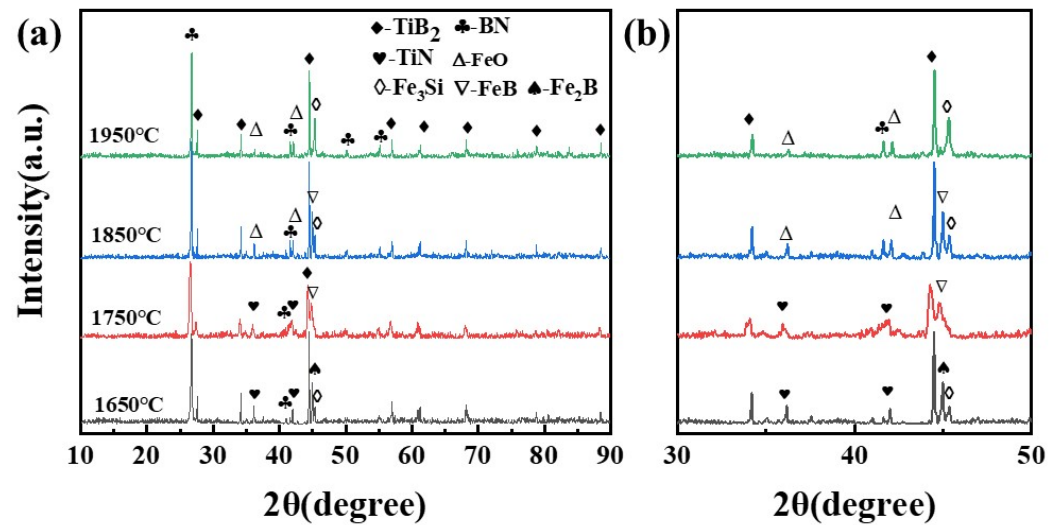
Figure 6. Properties of TiB$_2$-BN-SiC composite ceramics at various sintering temperatures: (**a**) apparent relative density, (**b**) electrical resistivity, (**c**) elastic modulus and bending strength, and (**d**) thermal conductivity and mean thermal expansion coefficient.

### 3.2.2. Influence of the Sintering Temperature on the Phase and Microstructure

Figure 7 shows that the diffraction peaks that correspond to TiB$_2$ and BN are detected in the samples that are fired at four temperatures, and the peak intensities of the two phases are more consistent among the temperatures. The peak width that corresponds to BN gradually narrows with increasing sintering temperature, thereby indicating that the BN powder has higher crystallization performance with increasing temperature and the corresponding BN matrix is purer. Various impurity peaks, such as FeO, Fe$_3$Si, and FeB peaks, are also detected in the 35–50° interval. As the temperature increases, the diffraction peaks of FeB and Fe$_2$B, among others, gradually disappear and are replaced by increasingly enhanced Fe$_3$Si peaks. This may be due to the increase in temperature accelerating the formation of the liquid phase, in which some of the Si atoms enter the Fe atoms to form Fe$_3$Si intermetallic compounds. Fe$_3$Si has excellent electrical properties [29]. Therefore, the sudden drop in resistivity of the composite ceramic at 1950 °C may be because the contents of FeO and Fe$_3$Si, which are conductive materials, in the sample have reached the threshold of percolation theory.

Figure 7. (**a**) XRD patterns of TiB$_2$-BN-SiC composite ceramics at different sintering temperatures, (**b**) is their local feature.

Figure 8 shows that the large grains in the figure are TiB$_2$ and SiC, and the flaky structure grains are BN. With increasing sintering temperature, the grains of the flaky BN ceramics grow significantly, the TiB$_2$ and SiC grains are dispersed around the BN, the two are more closely combined, and the voids are reduced. This is because at 1650 °C, the sintering temperature is low, the growth of BN grains is not complete, and the density is not high. Above 1750 °C, the densification process of BN grains is basically completed under the effect of B$_2$O$_3$ sintering. With a further increase in the sintering temperature, TiB$_2$, SiC, and BN grains grow more completely; hence, the apparent relative density increases. The growth of the grains of the lamellar BN causes more transgranular fractures of the lamellar structure at the ceramic fracture; thus, the bending strength of the sample increases, which is consistent with the result of Figure 6c.
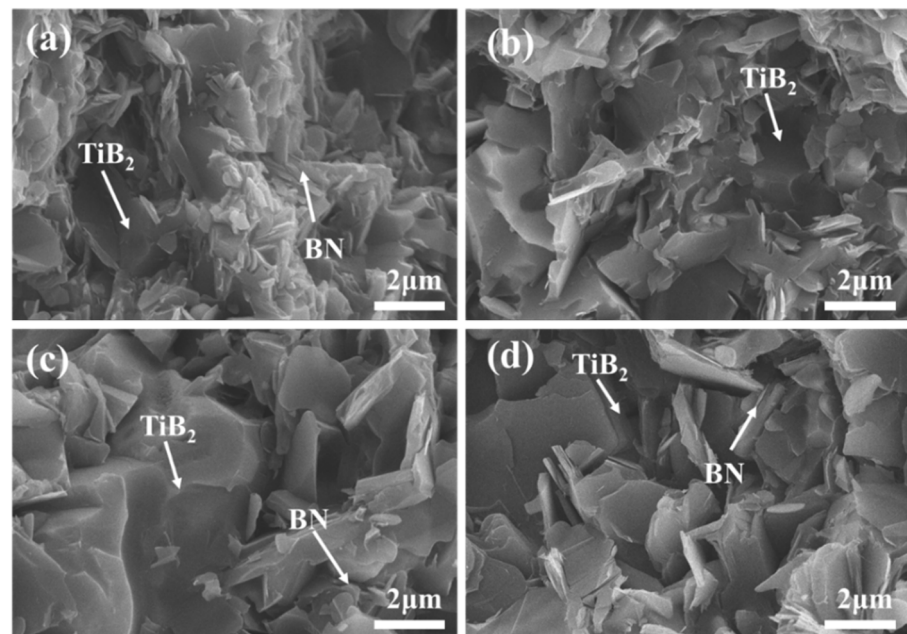
Figure 8. Cross-sectional SEM images of TiB$_2$-BN-SiC composite ceramics at four sintering temperatures: (**a**) 1650 °C, (**b**) 1750 °C, (**c**) 1850 °C, and (**d**) 1950 °C.

Figure 9 shows backscattered images of TiB_2-BN-SiC composite ceramics with four sintering temperatures. As the sintering temperature increases, the size of the white particles in the image gradually increases, and abnormal crystal grains are observed at 1950 °C. The particle size reaches from 5 µm in Figure 9a to 10 µm in Figure 9d, which is caused by overburning at sintering temperatures that are too high. As the content of each component is the same, it is found that the sintering temperature has little effect on the phase distribution of TiB_2-BN-SiC composite ceramics.
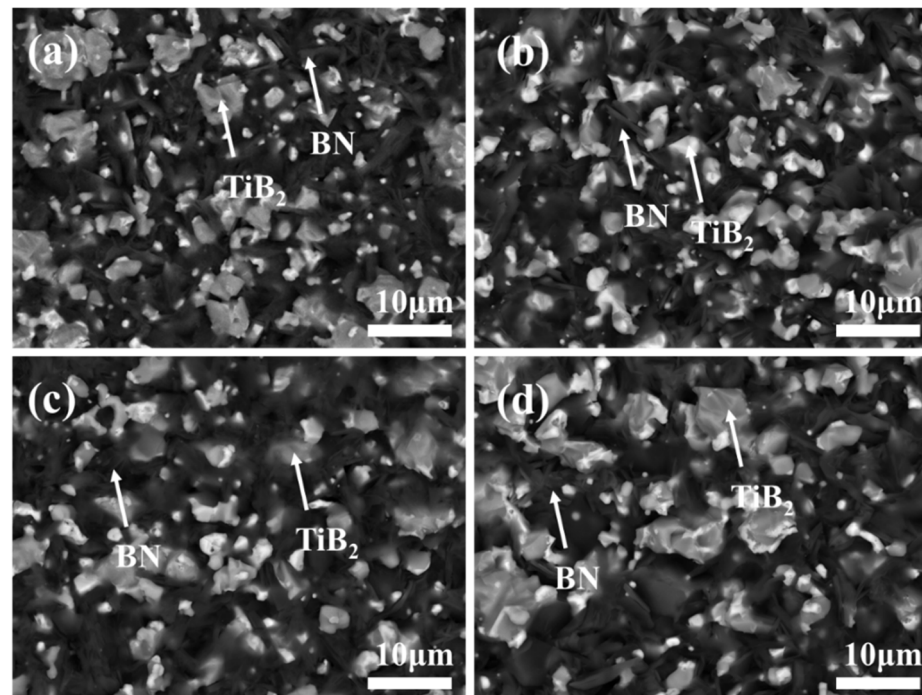
Figure 9. BSE images of TiB_2-BN-SiC composite ceramics at four sintering temperatures: (**a**) 1650 °C, (**b**) 1750 °C, (**c**) 1850 °C, and (**d**) 1950 °C.

After investigation, there are not many studies on TiB_2-BN-SiC composite ceramics, Xiaowei Yang [3] has studied similar systems, but there are big differences in the proportions of components [30]. It is widely proved that SiC can better adjust the sintering performance of TiB_2. Therefore, adding SiC to the TiB_2-BN two phases to improve part of the properties of TiB_2-BN ceramics can be better reflected in this study. However, due to the difficulty of sintering the covalent compound BN [31], the improvement of the ceramic density of this system still needs further research and exploration. The introduction of a certain liquid phase into the extremely difficult-to-densify boride ceramics to achieve liquid-phase sintering to promote densification still needs further exploration [32].

4. Conclusions

In this experiment, TiB_2-BN-SiC ternary composite ceramics with low resistivity and satisfactory thermal stability were prepared by the spark plasma sintering method after mechanically alloying the raw material powder. The following conclusions were obtained regarding the influence of various factors on the electrical properties, mechanical properties, thermal properties, phase, and microstructure of TiB_2-BN-SiC composite ceramics:

(a) As the ratio of TiB_2-SiC increases, the electrical resistivity of the TiB_2-BN-SiC composite ceramics decreases, the thermal conductivity and thermal expansion coefficient gradually increase, and the grain size of the ceramic cross-section increases significantly. When the ratio is increased from 3:1 to 12:1, the resistivity drops from 8000 to 5000 µΩ·cm; the thermal conductivity rises from 28.8 to 34.2 W/m·K; and the thermal expansion coefficient increases from 7.36×10^{-6}/K to 10.80×10^{-6}/K.

(b) The increase in the sintering temperature of the multiphase ceramics promotes the relative density and mechanical properties of the ceramics. The electrical resistance initially increases and subsequently decreases at 1950 °C. The thermal conductivity and thermal expansion also gradually increase.

(c) The small amount of Fe that is introduced in the process of mechanically alloying the composite powder reacts with the main powder and the impurities in the powder during the sintering process to produce FeB and FeO, among other products, and melts into a liquid phase at high temperature to promote the sintering of the ceramics. The earlier the liquid phase is formed, the higher the densification performance of the ceramic.

References

1. Wang, H.; Xu, M.; Ping, H.; Fu, Z. Large-scale synthesis and growth mechanism of boron nitride nanocomposite assembled by nanosheets and nanotubes. *J. Am. Ceram. Soc.* **2020**, *103*, 5594–5598. [CrossRef]

2. Nguyen, T.P.; Hamidzadeh Mahaseni, Z.; Dashti Germi, M.; Delbari, S.A.; Le, Q.V.; Ahmadi, Z.; Shokouhimehr, M.; Shahedi Asl, M.; Sabahi Namini, A. Densification behavior and microstructure development in TiB_2 ceramics doped with h-BN. *Ceram. Int.* **2020**, *46*, 18970–18975. [CrossRef]

3. Yang, X.; Chen, J.; Xing, R.; Babapoor, A. Hot-pressing and characterization of TiB_2–SiC composites with different amounts of BN additive. *Ceram. Int.* **2021**, *47*, 16652–16660. [CrossRef]

4. Nguyen, V.-H.; Delbari, S.A.; Sabahi Namini, A.; Ahmadi, Z.; Le, Q.V.; Shokouhimehr, M.; Shahedi Asl, M.; Mohammadi, M. Microstructural evolution of TiB_2–SiC composites empowered with Si_3N_4, BN or TiN: A comparative study. *Ceram. Int.* **2021**, *47*, 1002–1011. [CrossRef]

5. Nguyen, T.P.; Germi, M.D.; Mahaseni, Z.H.; Delbari, S.A.; Le, Q.V.; Ahmadi, Z.; Shokouhimehr, M.; Namini, A.S.; Asl, M.S. Enhanced densification of spark plasma sintered TiB_2 ceramics with low content AlN additive. *Ceram. Int.* **2020**, *46*, 22127–22133. [CrossRef]

6. Song, S.; Zhang, T.; Xie, C.; Zhou, J.; Li, R.; Zhen, Q. Growth behavior of TiB_2 hexagonal plates prepared via a molten-salt-mediated carbothermal reduction. *J. Am. Ceram. Soc.* **2020**, *103*, 719–723. [CrossRef]

7. Nguyen, V.-H.; Shahedi Asl, M.; Hamidzadeh Mahaseni, Z.; Dashti Germi, M.; Delbari, S.A.; Le, Q.V.; Ahmadi, Z.; Shokouhimehr, M.; Sabahi Namini, A.; Mohammadi, M. Role of co-addition of BN and SiC on microstructure of TiB_2-based composites densified by SPS method. *Ceram. Int.* **2020**, *46*, 25341–25350. [CrossRef]

8. Eichler, J.; Lesniak, C. Boron nitride (BN) and BN composites for high-temperature applications. *J. Eur. Ceram. Soc.* **2008**, *28*, 1105–1109. [CrossRef]

9. Dong, L.; Li, D.J.; Zhang, S.; Yan, J.Y.; Liu, M.Y.; Gao, C.K.; Wang, N.; Liu, G.Q.; Gu, H.Q.; Wan, R.X. Microstructure and mechanical properties of as-deposited and annealed TiB_2/BN superlattice coatings. *Thin Solid Films* **2012**, *520*, 5328–5332. [CrossRef]

10. McKinnon, R.; Grasso, S.; Tudball, A.; Reece, M.J. Flash spark plsma sintering of cold-Pressed TiB_2-hBN. *J. Eur. Ceram. Soc.* **2017**, *37*, 2787–2794. [CrossRef]

11. Wang, B.; Cai, D.; Xue, C.; Niu, B.; Yang, Z.; Duan, X.; Li, D.; Jia, D.; Zhou, Y. Preparation and mechanical properties of laminated B_4C–TiB_2/BN ceramics. *Ceram. Int.* **2021**, *47*, 31214–31221. [CrossRef]

12. Wang, H.; Xu, M.; Ping, H.; Fu, Z. Surface-diffusion mechanism for synthesis of substrate-free and catalyst-free boron nitride nanosheets. *J. Eur. Ceram. Soc.* **2020**, *40*, 5324–5331. [CrossRef]

13. Herrmann, M.; Räthel, J.; Höhn, S.; Eichler, J.; Michaelis, A. Interaction of titanium diboride/boron nitride evaporation boats with aluminium. *J. Eur. Ceram. Soc.* **2011**, *31*, 2401–2406. [CrossRef]

14. Bai, J.; Wang, Q.; Du, Q.; Zhang, Y.; Wei, C. Effects of ZrB_2 addition on properties of BN-AlN-TiB_2 composite ceramics. *Naihuo Cailiao* **2020**, *54*, 24–26. [CrossRef]

15. Zhang, W.; Chen, X.; Yamashita, S.; Kubota, M.; Kita, H. B_4C-SiC Ceramics with Interfacial Nanorelief Morphologies and Low Underwater Friction and Wear. *ACS Appl. Nano Mater.* **2021**, *4*, 3159–3166. [CrossRef]

16. Foong, L.K.; Xu, C. Hot pressing and microstructural characterization of SiC and TiN added TiB_2 ceramics. *Ceram. Int.* **2021**, *47*, 3946–3954. [CrossRef]

17. Tian, W.; Kita, H.; Hyuga, H.; Kondo, N.; Nagaoka, T. Reaction joining of SiC ceramics using TiB_2-based composites. *J. Eur. Ceram. Soc.* **2010**, *30*, 3203–3208. [CrossRef]

18. Zhu, Y.; Luo, D.; Li, Z.; Wang, Y.; Cheng, H.; Wang, F.; Chen, T. Effect of sintering temperature on the mechanical properties and microstructures of pressureless-sintered B_4C/SiC ceramic composite with carbon additive. *J. Alloys Compd.* **2020**, *820*, 153153. [CrossRef]

19. Qu, Z.; He, R.; Cheng, X.; Fang, D. Fabrication and characterization of B_4C–ZrB_2–SiC ceramics with simultaneously improved high temperature strength and oxidation resistance up to 1600 °C. *Ceram. Int.* **2016**, *42*, 8000–8004. [CrossRef]

20. Ping, H.; Wang, G.L.; Zhi, W. Oxidation mechanism and resistance of ZrB_2-SiC composites. *Corros. Sci.* **2009**, *51*, 2724–2732. [CrossRef]

21. He, Q.; Tian, S.; Xie, J.; Xiang, C.; Wang, H.; Wang, W.; Fu, Z. Microstructure and anisotropic mechanical properties of B6.5C-TiB_2-SiC-BN composites fabricated by reactive hot pressing. *J. Eur. Ceram. Soc.* **2020**, *40*, 2862–2869. [CrossRef]

22. Prashanth, M.; Karunanithi, R.; RasoolMohideen, S.; Sivasankaran, S. A comprehensive exploration on the development of nano Y_2O_3 dispersed in AA 7017 by mechanical alloying and hot-pressing technique. *Ceram. Int.* **2021**, *47*, 22924–22938. [CrossRef]

23. Xia, W.; Zarezadeh Mehrizi, M. Direct synthesis of NiAl intermetallic matrix composite with TiC and Al_2O_3 reinforcements by mechanical alloying of NiO–Al–Ti–C powder mixture. *Ceram. Int.* **2021**, *47*, 26863–26868. [CrossRef]

24. Jimba, Y.; Kondo, S.; Yu, H.; Wang, H.; Okuno, Y.; Kasada, R. Effect of mechanically alloyed sintering aid on sinterability of TiB_2. *Ceram. Int.* **2021**, *47*, 21660–21667. [CrossRef]

25. Wang, Y.; Fu, Z.; Wang, W.; Zhang, J. Numerical simulation of the temperature field in sintering of TiB_2-BN by SPS. *J. Wuhan Univ. Technol.-Mater. Sci. Ed.* **2006**, *21*, 126–128. [CrossRef]

26. Keller, A.R.; Zhou, M. Effect of Microstructure on Dynamic Failure Resistance of Titanium Diboride/Alumina Ceramics. *J. Am. Ceram. Soc.* **2003**, *86*, 449–457. [CrossRef]

27. Chlup, Z.; Bača, Ľ.; Halasová, M.; Neubauer, E.; Hadraba, H.; Stelzer, N.; Roupcová, P. Effect of metallic dopants on the microstructure and mechanical properties of TiB_2. *J. Eur. Ceram. Soc.* **2015**, *35*, 2745–2754. [CrossRef]

28. Tian, S. Fabrication and Characteristics of TiB_2-BN-SiC Composite Ceramics. Master's Thesis, Wuhan University of Technology, Wuhan, China, 2011.

29. Kalita, M.P.C.; Peramal, A.; Srinivasan, A. Structural analysis of mechanically alloyed nanocrystalline $Fe_{75}Si_{15}Al_{10}$ powders. *Mater. Lett.* **2007**, *61*, 824–826. [CrossRef]

30. Song, B.; Yang, W.; Liu, X.; Chen, H.; Akhlaghi, M. Microstructural characterization of TiB_2–SiC–BN ceramics prepared by hot pressing. *Ceram. Int.* **2021**, *47*, 29174–29182. [CrossRef]

31. Wang, N.; Dong, L.; Gao, C.K.; Li, D.J. A study of structure, energy and electronic properties of TiB_2/c-BN interface by first principles calculations. *Opt. Mater.* **2014**, *36*, 1459–1462. [CrossRef]

32. Son, H.W.; Berthebaud, D.; Yubuta, K.; Yoshikawa, A.; Shishido, T.; Suzuta, K.; Mori, T. New Synthesis Route for Complex Borides; Rapid Synthesis of Thermoelectric Yttrium Aluminoboride via Liquid-Phase Assisted Reactive Spark Plasma Sintering. *Sci. Rep.* **2020**, *10*, 8914. [CrossRef] [PubMed]